Available online at www.sciencedirect.com
SCIENCE DIRECT®
Organic Electronics 4 (2003) 21–26
Organic Electronics
www.elsevier.com/locate/orgel

A low drive voltage, transparent, metal-free n–i–p electrophosphorescent light emitting diode

M. Pfeiffer [a,b,*], S.R. Forrest [a,*], X. Zhou [b], K. Leo [b]

[a] Department of Electrical Engineering, Princeton University, Center for Photonics & Optoel. Mat., Princeton, NJ 08544, USA
[b] Institut für Angewandte Photophysik (IAPP), Technische Universität Dresden, George-Baehr Strasse 1, D-01062 Dresden, Germany

Received 4 October 2002; received in revised form 27 January 2003; accepted 6 February 2003

Abstract

We demonstrate a transparent, inverted, electrophosphorescent n–i–p organic light emitting diode (OLED) exhibiting a luminance of 500 cd/m^2 at 3.1 V, and with a luminous power efficiency of 23 lm/W when light emitted from both top and bottom surfaces is summed. We find that 10% more light is emitted from the top surface; hence a power efficiency of 12 lm/W is obtained for a device viewed through the top, transparent contact. This device, with applications to head-up and displays employing n-type Si driver circuitry, has significantly higher power efficiency and lower drive voltage than undoped fluorescent inverted OLEDs. Efficient injection of both electrons and holes is made possible by controlled n- and p-doping of the transport layers with high doping levels. The light emitting region is protected from ITO sputtering damage by a 210 nm thick p-doped hole transport layer. The transparency of the device at the peak OLED emission wavelength of 510 nm is $(80 \pm 5)\%$.

Keywords: Transparent organic light emitting diodes; Doping; Electrophosphorescence

1. Introduction

The use of organic light emitting diodes (OLEDs) is considered a promising approach for the realization of flat panel displays due to their saturated and bright color rendition of images, large viewing angle, high power efficiency and ability to provide full motion video [1,2]. Typically, OLEDs are prepared on transparent, conductive substrates made from glass or polymer foils coated with indium–tin–oxide (ITO) that serves as the transparent anode. Then, a stack of organic layers is deposited, starting with a hole transport layer (HTL), followed by a light emission layer (EML), an electron transport layer (ETL) and a metallic, reflective cathode. However, for active matrix displays, it is desirable that the organic stack be directly deposited onto the silicon-based drive circuitry. Since the active matrix is light-absorbing, to ensure a large display aperture ratio, it is desirable that the top contact of the OLED be transparent [3]. Furthermore, compatibility with the Si electronics (typically having n-channel transistors) requires that, in this configuration, the electron

* Corresponding authors. Address: Institut für Angewandte Photophysik (IAPP), Technische Universität Dresden, George-Baehr Strasse 1, D-01062 Dresden, Germany (M. Pfeiffer). Tel.: +1-609-258-4532; fax: +1-609-258-7272 (S.R. Forrest).
E-mail addresses: pfeiffer@iapp.de (M. Pfeiffer), forrest@ee.princeton.edu (S.R. Forrest).

1566-1199/03/$ - see front matter
doi:10.1016/S1566-1199(03)00004-1

injection occurs from the substrate contact. In this case, the organic layer sequence is inverted to allow for efficient electron injection into the ETL. Accordingly, considerable efforts have aimed at the realization of both transparent OLEDs [4–9] and organic inverted LEDs (OILEDs) [10,11].

A particular challenge in realizing a transparent OLED is to prepare a transparent and efficiently carrier injecting top contact by sputter deposition of ITO without damaging the organics in the EML. For example, Gu et al. [4] reported that at least 7.5 nm Mg:Ag has to be inserted between the organics and the sputtered ITO to avoid device shorts, which reduces the transparency to ~60%. Alternatively, optical losses can be reduced by replacing the metal with a thermally stable organic material such as copper phthalocyanine (CuPc) [5,6], 3,4,9,10-perylenetetracarboxylic dianhydride [11] or metal acethylacetonate complexes ([Mt(acac)$_2$]) [9]. Unfortunately, this can lead to reduced electron injection efficiency, and hence higher operating voltages [5]. This problem can be partially overcome by incorporating lithium in the organic/ITO cathode interface region [6,8]. For example, a conventional tris(8-hydroxyquinoline) aluminium (Alq_3)-based OLED with a dimethyl-diphenyl phenanthroline (BCP)/Li/ITO cathode exhibits a transparency of ~90% and an external quantum efficiency of 1%, although the drive voltage was ~9 V at a current density of 10 mA/cm^2 [8].

These injection problems are even more pronounced in OILEDs, where the organic materials are deposited onto the cathode (opposite to the case of conventional anode-side down devices where the cathode is deposited onto the organic layers), leading to high operating voltages and low quantum efficiencies as compared with conventional OLEDs [11]. These problems have been overcome by Zhou et al. [12] who reported a semitransparent OILED with low driving voltage (4 V for 100 cd/m^2) and an external quantum efficiency of 0.8% based on an inverted (i.e. n–i–p versus p–i–n) structure [13] that makes use of efficient electron injection from the ITO bottom contact into Li doped diphenyl-phenanthroline (BPhen). Thin undoped blocking layers adjacent to the doped transport layers are needed to achieve high efficiency [14]. For the HTL, a thick layer of p-doped m-MTDATA was employed, along with a 10 nm thick semitransparent Au anode.

Extending this approach to phosphorescent emitters and fully transparent anode contacts, here we demonstrate a transparent, metal free electrophosphorescent [15,16] OILED with a quantum efficiency (when the output is summed from both top and bottom emitting surfaces) of up to 8% and a drive voltage of 2.9 V at 100 cd/m^2, corresponding to a luminous power efficiency >20 lm/W up to 1500 cd/m^2.

2. Experimental

The n–i–p OILEDs are prepared on a solvent cleaned and ozone treated ITO coated glass substrate. The ITO serves as a transparent cathode with a sheet resistance of 20 Ω/sq. The thin films are deposited by vacuum thermal evaporation in a chamber with a base pressure of 10^{-7} Torr. All organic materials except the acceptor dopant, 2,3,5,6-tetrafluoro-7,7,8,8-tetracyano-quinodimethane (F_4-TCNQ), were purified by vacuum gradient sublimation. Doping is by co-evaporation from independent sources whose effusion rates are monitored using a quartz crystal microbalance. Firstly, a 15 nm thick layer of BPhen doped with Li [17] (≈1 atom/molecule) are deposited as the conductive electron injection and transport layer. The Li was stored in mineral oil and washed with dimethyl sulfoxide immediately prior to insertion into the vacuum chamber to avoid oxidation. To prevent quenching of excitons by the Li dopants, a 20 nm thick buffer layer [13] of undoped BPhen is deposited, followed by the 10 nm thick EML consisting of 4,4′-N,N′-dicarbazol-biphenyl (CBP) doped with 7 wt.% of the green phosphor, tris-(phenylpyridine) iridium ($Ir(ppy)_3$). Next, a 15 nm thick undoped buffer layer of tris-(phenylpyrazole) iridium ($Ir(ppz)_3$) is deposited. Having a wide energy gap and higher singlet and triplet exciton energies than the materials comprising the EML [18], $Ir(ppz)_3$ efficiently blocks electrons from penetrating into the p-doped HTL while also confining excitons in the EML [19].

To complete the n–i–p structure, a p-doped HTL is deposited consisting of a 200 nm thick

layer of 4,4′,4″-tris-(3-methylphenylphenylamino)-triphenylamine (m-MTDATA) [20] and a 20 nm "sputter damage protection" layer [5,11] of copper phthalocyanine (CuPc), both doped with approximately 2 mol% F_4-TCNQ, which has been shown to be an efficient acceptor for both materials [21]. Finally, the anode is prepared by radio frequency (RF)-magnetron sputtering of a 60 nm thick layer of ITO at a deposition rate of 3 nm/min with an RF power of 57 W in 2 mTorr of Ar.

To measure the EL intensity, the OLEDs are placed directly on the surface of a large area, calibrated silicon photodiode capturing only light emitted in the forward direction through the bottom ITO contact. For the transparent devices, the ratio of top-to-bottom emission was determined to be 1.1 ± 0.1. The efficiencies and luminances reported for transparent devices are the sum of top and bottom emission for comparison with non-transparent devices where the bottom emission includes that reflected from the top contact.

3. Results and discussion

In Fig. 1, the performance of an electrophosphorescent n–i–p OILED (sample A) is compared to that of a conventional electrophosphorescent OLED with the layer sequence glass substrate/ITO/N,N′-diphenyl-N,N′-bis(1-naphthylphenyl)-1,1′-biphenyl-4,4′-diamine (α-NPD) (50 nm)/CBP:7% $Ir(ppy)_3$/BCP(10 nm)/Alq_3 (40 nm)/LiF (0.5 nm)/Al (100 nm) (sample B) as reported by Adachi et al. [22]. Although the n–i–p OILED employs the same material, namely ITO, as both the anode and cathode, its luminance–voltage characteristic is considerably steeper than for the conventional OLED using ITO as the anode and LiF/Al as an efficient cathode material. The n–i–p-device reaches 100 cd/m^2 at 3 V, and 1000 cd/m^2 at 3.5 V, as compared to 4 and 5 V, respectively, for the OLED.

The external quantum efficiency versus luminance, plotted in Fig. 2, is considerably lower for the OILED than for the OLED at low intensities, although this difference significantly decreases with brightness. For example, above 250 cd/m^2, the luminance power efficiency, also shown in Fig. 2,

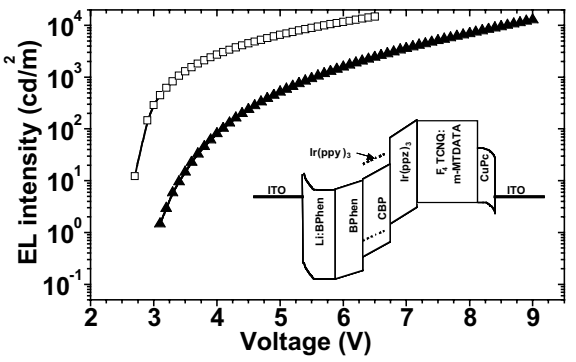

Fig. 1. Electroluminescence (EL) intensity versus applied voltage for CBP:$Ir(ppy)_3$ based electrophosphorescent OLEDs. Open squares: inverted transparent n–i–p OILED (sample A) measured as the sum of the light emitted through the top and bottom contacts. Triangles: conventional OLED reference sample with undoped transport layers and a reflecting top contact (sample B) as in [22]. Inset: proposed equilibrium energy level diagram of the inverted transparent n–i–p OLED.

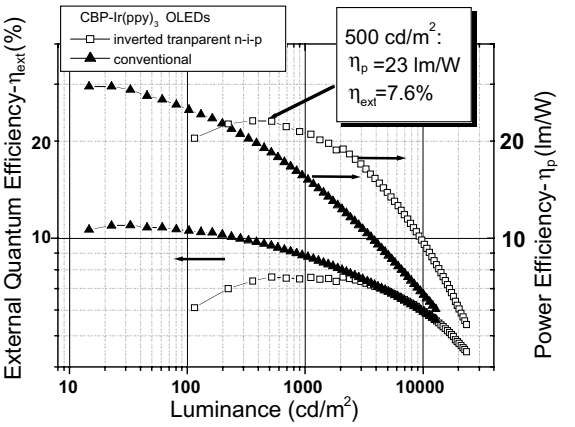

Fig. 2. External quantum efficiency and luminous power efficiency versus luminance for sample A, a transparent n–i–p OILED (open squares), compared with sample B, a conventional electrophosphorescent OLED. Here, the luminance is the sum of the light emitted from both the top and bottom device surfaces.

of the transparent OILED exceeds that of the OLED due to its lower drive voltage. At a brightness of 500 cd/m^2, the n–i–p OILED power efficiency is 23 lm/W.

The current versus voltage (I–V) characteristics of samples A and B, along with that of a conventional p–i–n electrophosphorescent OLED

(sample C) with the layer sequence glass/ITO/m-MTDATA:2 mol% F_4-TCNQ (50 nm)/Ir(ppz)$_3$ (10 nm)/CBP:7 wt.% Ir(ppy)$_3$ (5 nm)/BPhen (25 nm)/Bphen:Li (40 nm)/Al are shown in Fig. 3. The performance of the latter device is discussed in [19]. Additionally, the characteristics of an inverted device (sample A*) otherwise identical with sample A but with Au, instead of ITO as the anode, is shown. For all doped structures, the characteristics are shifted substantially to lower voltages relative to the conventional electrophosphorescent OLED with undoped transport layers. Comparing only the doped OLEDs, the increase in voltage of the inverted as compared with the conventional devices in the low current region between 10 μA/cm^2 and 1 mA/cm^2 is only ~0.2 V, indicating that the injection barriers for both carrier types are low in the OILED. This is an anticipated result of doping near contacts, which leads to sharp band bending in that region. This, in turn, leads to efficient electron and hole tunneling across the narrowed contact barriers into the ETL and HTL, respectively.

As shown in the proposed equilibrium energy level diagram in the inset of Fig. 1, the n–i–p-structures include high internal energy barriers that prevent the injection of minority carriers from the EML into the transport layers, which generally leads to reduced exciton generation. That is, the lowest unoccupied molecular orbital offset from CBP to Ir(ppz)$_3$ is at least 1 eV [18], and the highest occupied molecular orbital offset from CBP to BPhen is ~0.7 eV [15]. These barriers ensure that carriers recombine in the EML due to the nearly equal number of holes and electrons injected into that energetically confined region. Accordingly, high currents are only possible if injection is efficient for *both* carrier types. The maximum external quantum efficiency, corresponding to an internal quantum efficiency of ~40% [16] is consistent with our conclusion of efficient bipolar injection.

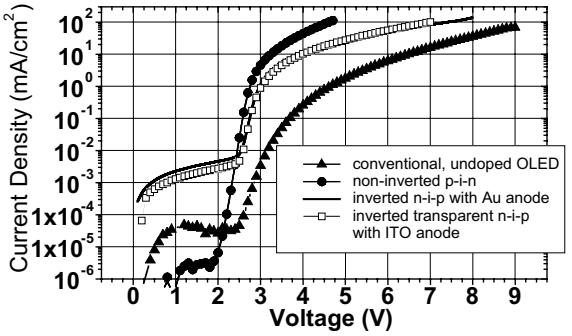

Fig. 3. Current–voltage characteristics of several CBP:Ir(ppy)$_3$ electrophosphorescent OLEDs. Open squares: transparent n–i–p OILED (sample A). Black line: n–i–p OILED with Au as a top contact (sample A*). Triangles: conventional OLED (sample B). Circles: non-inverted p–i–n OLED with reflecting top contact (sample C).

The difference in the operating voltage between the non-inverted and the inverted doped structures increases from 0.3 V at 1 mA/cm^2 to ~1 V at 10 mA/cm^2. This increasing difference is attributed to the larger thickness of the doped m-MTDATA layer in the inverted device. Here, the increase of 0.7 V approximately corresponds to the voltage drop across 150 nm thick m-MTDATA doped with 2% F_4-TCNQ at a current density of 10 mA/cm^2, assuming a conductivity of about 0.3 μS/cm [23]. On the other hand, the calculated voltage drop across the doped HTL is <0.1 V for currents <1 mA/cm^2, i.e. the increased thickness of the inverted device will not significantly increase the voltage needed in active matrix displays.

Significant differences in the I–V-characteristics between the inverted and non-inverted doped OLEDs only appear at voltages where no light emission is observed (<2.4 V), and the leakage current is dominated by shunt paths. The leakage current, however, is larger in the inverted structure, making this structure less suitable for passive matrix displays. We attribute this to insufficient wetting of the ITO with BPhen. We have observed that a neat layer of BPhen on glass or ITO crystallizes within a few hours after deposition. To achieve devices with long term stability, therefore, more stable materials than BPhen are required.

The I–V characteristics of the n–i–p OILED demonstrate the effects of doping. First, doping reduces ohmic losses in the bulk of the transport layers [14], enabling the use of a thick HTL to protect the sensitive active region from defects induced by sputter deposition of the ITO anode. Indeed, the overall thickness of the organic layers in the n–i–p structure is 250 nm, which would lead to considerably higher driving voltages in undoped

devices. Second, doping improves carrier injection over high energy barriers [13]. For the inverted device, efficient injection is obtained for both electrodes, in spite of large energy barriers. For the cathode, the difference between the ITO work function and the electron affinity of BPhen presents a barrier height >1.5 eV [24]. Further, hole injection from ITO usually requires pre-treatment of the ITO surface by ozone or an oxygen plasma to increase its work function [25]. Such treatment is not possible for the interface between organic layers and the ITO on the top diode surface. For example, Blochwitz et al. [26] have shown that a Schottky junction is formed at the interface between zinc phthalocyanine (ZnPc) and untreated ITO. However, the depletion region at the junction becomes thinner than 5 nm upon doping the ZnPc with 2 mol% F_4-TCNQ, allowing holes to tunnel through the barrier. A similar mechanism is possibly responsible for the efficient injection of holes from ITO into the highly doped transport layers of the present device, as found previously for non-inverted OLEDs [14].

The transparency spectrum of the n–i–p OILED, as shown in Fig. 4, shows a transmission of $(80 \pm 5)\%$ at 510 nm, the peak emission wavelength of $Ir(ppy)_3$, coinciding with the transparency window of the CuPc absorption. The transparency is reduced to about 60% at the first absorption peak of CuPc (700 nm). Also shown in the figure is the transmission of the device in the absence of the ITO anode, which differs somewhat at both short and long wavelengths from that of a full device that includes the contact. Given that the transmission is higher for the device with the anode, we speculate that the difference is primarily due to enhanced outcoupling of light due to microcavity effects resulting from the presence of the ITO.

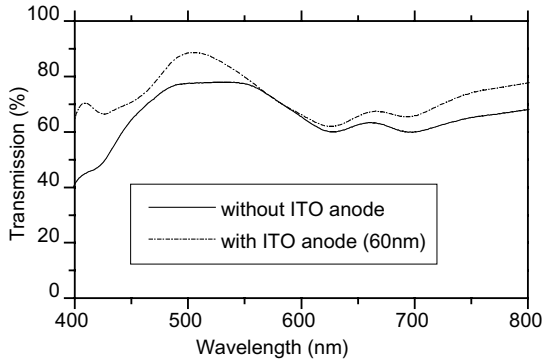

Fig. 4. Optical transmission spectrum of the transparent n–i–p OILED (sample A) with and without a sputter deposited ITO top contact.

4. Conclusions

In summary, we have demonstrated a transparent, metal free, inverted electrophosphorescent n–i–p OILED for use in top emitting active matrix and transparent displays. The n–i–p structure exhibits a drive voltage comparable to that obtained using a conventional p–i–n architecture in spite of high energy barriers at both contacts. A high quantum efficiency is obtained by using a thin electrophosphorescent emission layer (EML) with buffer layers that ensure that charge carriers and excitons are confined in the EML. The 80% transparent (at a wavelength of 510 nm) OILED reaches a luminous power efficiency of up to 23 lm/W when light output from both top and bottom transparent contacts is summed. These results suggest that the n–i–p architecture, combined with the use of electrophosphorescent emitters, have potential applications for a new generation of efficient top emitting displays on silicon-based drive circuitry, as well as transparent OLEDs for use in large area and head-mounted displays.

Acknowledgements

The authors thank the Defense Advanced Research Projects Agency, Universal Display Corp., the German Secretary for Education and Research, BMBF and the German Research Foundation, DFG for support of this work. We also thank Prof. Mark Thompson and his team at the University of Southern California for supplying $Ir(ppz)_3$.

References

[1] C.W. Tang, S.A. VanSlyke, Appl. Phys. Lett. 51 (12) (1987) 913–915.
[2] S. Miyata, H.S. Nalwa (Eds.), Organic Electroluminescent Materials and Devices, Gordon and Breach Science Publishers, Amsterdam, 1997.
[3] V. Bulovic, G. Gu, P.E. Burrows, M.E. Thompson, S.R. Forrest, Nature 380 (1996) 29.
[4] G. Gu, V. Bulovic, P.E. Burrows, S.R. Forrest, M.E. Thompson, Appl. Phys. Lett. 68 (1996) 2606.
[5] G. Parthasarathy, P.E. Burrows, V. Khalfin, V.G. Kozlov, S.R. Forrest, Appl. Phys. Lett. 72 (1998) 2138.
[6] L.S. Hung, C.W. Tang, Appl. Phys. Lett. 74 (1999) 3209.
[7] P.E. Burrows, G. Gu, S.R. Forrest, E.P. Vicenzi, T.X. Zhou, J. Appl. Phys. 87 (2000) 3080.
[8] G. Parthasarathy, C. Adachi, P.E. Burrows, S.R. Forrest, Appl. Phys. Lett. 76 (2000) 2128.
[9] A. Yamamori, S. Hayashi, T. Koyama, Y. Taniguchi, Appl. Phys. Lett. 78 (2001) 3343.
[10] D.R. Baigent, R.N. Marks, N.C. Greenham, R.H. Friend, S.C. Moratti, A.B. Holmes, Appl. Phys. Lett. 65 (1994) 2636.
[11] V. Bulovic, P. Tian, P.E. Burrows, M.R. Gokhale, S.R. Forrest, M.E. Thompson, Appl. Phys. Lett. 70 (1997) 2954.
[12] X. Zhou, M. Pfeiffer, J.S. Huang, J. Blochwitz-Nimoth, D.S. Qin, A. Werner, J. Drechsel, B. Maennig, K. Leo, Appl. Phys. Lett. 81 (2002) 922.
[13] J. Huang, M. Pfeiffer, A. Werner, J. Blochwitz, Sh. Liu, K. Leo, Appl. Phys. Lett. 80 (2002) 139.
[14] X. Zhou, M. Pfeiffer, J. Blochwitz, A. Werner, A. Nollau, T. Fritz, K. Leo, Appl. Phys. Lett. 78 (2001) 410.
[15] M.A. Baldo, S. Lamansky, P.E. Burrows, M.E. Thompson, S.R. Forrest, Appl. Phys. Lett. 75 (1999) 4.
[16] C. Adachi, M.A. Baldo, M.E. Thompson, S.R. Forrest, J. Appl. Phys. 90 (2001) 5048.
[17] J. Kido, T. Matsumoto, Appl. Phys. Lett. 73 (1998) 2866.
[18] M.E. Thompson, C. Adachi, unpublished results.
[19] M. Pfeiffer, S.R. Forrest, K. Leo, M.E. Thompson, Adv. Mater. 14 (2002) 1633.
[20] Y. Shirota, Y. Kuwabara, D. Okuda, R. Okuda, H. Ogawa, H. Inada, T. Wakimoto, H. Nakada, Y. Yonemoto, S. Kawami, K. Imai, J. Lumin. 72–74 (1997) 985.
[21] B. Maennig, M. Pfeiffer, A. Nollau, X. Zhou, P. Simon, K. Leo, Phys. Rev. B 15 (64) (2001) 195208.
[22] C. Adachi, R. Kwong, S.R. Forrest, Org. Electron. 2 (2001) 37.
[23] J. Drechsel, M. Pfeiffer, X. Zhou, A. Nollau, K. Leo, Synth. Met. 127 (2002) 201.
[24] G. Parthasarathy, C. Shen, A. Kahn, S.R. Forrest, J. Appl. Phys. 89 (9) (2001) 4986.
[25] T.A. Beierlein, W. Brutting, H. Riel, E.I. Haskal, P. Muller, W. Riess, Synth. Met. 111 (2000) 295.
[26] J. Blochwitz, T. Fritz, M. Pfeiffer, K. Leo, D.M. Alloway, P.A. Lee, N.R. Armstrong, Organic Electronics 2 (2001) 97.